AIAA JOURNAL
Vol. 30, No. 4, April 1992

Flux-Difference Split Algorithm for Unsteady Thin-Layer Navier-Stokes Solutions

L. Bruce Simpson*
U.S. Air Force Wright Laboratory, Eglin Air Force Base, Florida 32542
and
David L. Whitfield†
Mississippi State University, Mississippi State, Mississippi 39762

An efficient flux-difference split scheme for calculating steady and unsteady thin-layer Navier-Stokes solutions for airfoils and wings is presented. Steady solutions for a flat plate laminar boundary-layer profile are correctly modeled with only three grid cells internal to the boundary layer. The flux-difference split algorithm was used to evaluate the scheme for unsteady viscous calculations. The diffusive terms are time lagged in the solution process. The scheme is second-order accurate in space and first-order accurate in time due to the explicit treatment of the diffusive terms. A Newton subiteration technique was implemented to allow for larger time step sizes and second-order temporal accuracy. The subiterations are more efficient than a normal time step iteration since the flux Jacobians need not be updated for the subiterations. The result is a more efficient and robust unsteady thin-layer Navier-Stokes algorithm that shows extremely good comparison with unsteady experimental data for oscillating airfoils and wings, even for calculations using large Courant numbers (up to 45,000) on extremely fine viscous grids. Engineering solutions for oscillating airfoils and wings can be obtained using the algorithm presented. Accurate viscous results can be obtained at a cost near that of inviscid results (on the same grid), yet with the inclusion of the time-lagged viscous terms, the results are superior to those obtained using inviscid schemes.

Introduction

THE area of computational fluid dynamics (CFD) has seen tremendous progress in recent years due to improvements in both computational algorithms and computer hardware. The improvements now make it possible to obtain steady inviscid solutions for very complex configurations such as modern fighter aircraft and the external weapons used on these aircraft.[1] However, many of these aircraft and weapons operate in flow conditions that make inviscid solutions an inappropriate model. Modern fighter aircraft must be able to release stores and missiles while maneuvering at transonic speeds. The analysis of these problems requires unsteady calculations, as does the analysis of aeroelastic problems. Often, solutions that include the effects of viscosity are necessary to appropriately model these flowfields; however, for these types of configurations, viscous solutions are not practical with current CFD codes due to the large computer run times and large memory requirements. The objective of the present work is to develop a three-dimensional unsteady viscous computational technique, whereby the magnitude of the time step that can be used is restricted by the physics of the flow being solved and not the numerics of the computational scheme used. To this end, a numerical scheme is presented that is shown to be accurate and computationally efficient enough to make viscous calculations practical for both steady and unsteady flowfields on extremely fine viscous grids.

The approach taken is an extension of two implicit Euler algorithms described by Belk[2] and Whitfield et al.[3] The algorithm used in this work is a combination of a flux-vector split (FVS) scheme based on Steger-Warming[4] splitting and a flux-difference split (FDS) scheme based on Roe's[5] approximate Riemann solver. The algorithm uses the implicit portion of the FVS scheme and the explicit portion of the FDS scheme. Since the algorithm behaves as a Roe-type scheme, it will be referred to here as an FDS or Roe scheme. The inclusion of the viscous terms into these Euler algorithms is accomplished as described by Gatlin,[6] where the diffusive terms have been added to the algorithm explicitly in order to save the cost of computing and storing the viscous flux Jacobians. The explicit treatment of the diffusive terms also preserves the computational efficiency peculiar to the inviscid algorithm.[2]

The three-dimensional Navier-Stokes equations in differential form are placed in curvilinear coordinates, and the thin-layer assumption is applied to reduce the Navier-Stokes equation set. The FDS scheme is presented in detail by Simpson[7] and only a short discussion is presented here. The FVS algorithm has been presented in some detail by Whitfield[8] (for stationary grids) and Belk[2] (for dynamic grids) and, therefore, is not discussed here. The FVS algorithm has been used by many people to obtain solutions for the Euler equations that compare well with experimental data for both steady and unsteady transonic flow problems. Lijewski[9] has shown excellent steady results for a complex canard-body-tail configuration at transonic Mach numbers and moderate range of incidence angles, whereas Belk and Whitfield[10] have shown unsteady results for oscillating airfoils and wings. However, Gatlin[6] and van Leer et al.[11] have shown that in some cases the FVS scheme is too dissipative to give good numerical results for viscous calculations, especially in high gradient regions such as boundary layers. Recent works by van Leer et al.,[11] Chakravarthy and Osher,[12] and many others have discussed implementations of the FDS scheme. However, Whitfield et al.[3] and Janus[13] have described a hybrid Roe algorithm that has been used to obtain excellent inviscid results for complex flowfields.[14]

Steady results were obtained for transonic Mach numbers and moderate range of incidence angles for a laminar flat plate,

Presented as Paper 89-1995 at the AIAA 9th Computational Fluid Dynamics Conference, Buffalo, NY, June 14–16, 1989; received April 16, 1990; revision received May 13, 1991; accepted for publication May 15, 1991.

*Acting Chief Aerodynamics Branch, Armament Directorate. Senior Member AIAA.
†Professor of Aerospace Engineering. Member AIAA.

RAE 2822 airfoil, the ONERA M6 wing, and the Langley rectangular planform supercritical (LRPS) wing. A comparison between the FVS and FDS algorithms for all combinations of flux limiters was obtained for steady flow, and all solutions were compared with experimental data. In the interest of space saving, only flat plate and LRPS results are shown here.

One of the major problems with unsteady thin-layer Navier-Stokes (TLNS) calculations is the severe time step size limitations that must be imposed to maintain a reasonable Courant-Friedrichs-Lewy (CFL) number. Efforts to execute the unsteady TLNS code for oscillating airfoils and wings using very large CFL numbers are discussed. In order to maintain stability at these large CFL numbers, a form of subiterations similar to those described by Rai and Chakravarthy[15] has been implemented. The result of subiterations is to converge the solution at a given time step before proceeding to the next step, thus eliminating linearization and factorization errors and increasing the stability. Unsteady results for both oscillating airfoils and wings in transonic flow and a moderate range of angles of attack are presented. The oscillating airfoil case (NACA 0012) is compared for various time steps sizes and numbers of subiterations, whereas the oscillating wing (LRPS) results are compared with the inviscid results of Belk[2] and experimental data.

Equations of Fluid Dynamics

The compressible, three-dimensional, time-dependent Navier-Stokes equations in strong conservation form (without body forces or external heat addition) can be written in body-fitted curvilinear coordinates defined by

$$\xi = \xi(x, y, z, t) \tag{1a}$$

$$\eta = \eta(x, y, z, t) \tag{1b}$$

$$\zeta = \zeta(x, y, z, t) \tag{1c}$$

$$\tau = \tau(t) \tag{1d}$$

After applying the coordinate transformation given in Eqs. (1), the three-dimensional Navier-Stokes equations become

$$\frac{\partial Q}{\partial \tau} + \frac{\partial (F_i - F_v)}{\partial \xi} + \frac{\partial (G_i - G_v)}{\partial \eta} + \frac{\partial (H_i - H_v)}{\partial \zeta} = 0 \tag{2}$$

where the vectors with i subscripts are the inviscid flux vectors and those with v subscripts are the viscous flux vectors. If all shearing surfaces are assumed to lie on constant η coordinate lines, then after making the thin-layer assumption,[16] which is based on neglecting all stress terms except those with derivatives tangent to the shearing surface, the result is the TLNS equations

$$\frac{\partial Q}{\partial \tau} + \frac{\partial F_i}{\partial \xi} + \frac{\partial (G_i - S_v)}{\partial \eta} + \frac{\partial H_i}{\partial \zeta} = 0 \tag{3}$$

where S_v is the viscous flux vector after making the thin-layer assumption.

Flux Difference Split Algorithm

An implicit, finite volume discretization of Eq. (3) with the viscous terms separated and moved to the right side becomes (note that subscript i has been dropped from the inviscid flux vectors)

$$\frac{\Delta Q^n}{\Delta \tau} + \frac{\delta F^{n+1}}{\Delta \xi} + \frac{\delta G^{n+1}}{\Delta \eta} + \frac{\delta H^{n+1}}{\Delta \zeta} = \frac{\delta S_v^{n+1}}{\Delta \eta} \tag{4}$$

However, instead of the usual second-order linearization of Briley-McDonald[17] or Beam-Warming,[18] the viscous terms are linearized as

$$S_v^{n+1} = S_v^n + \mathcal{O}(\Delta \tau) \tag{5}$$

The remaining fluxes are split according to the sign of their eigenvalues, linearized, and then factored into two terms as

$$[I + \Delta\tau(\delta_\xi A^+ \times + \delta_\eta B^+ \times + \delta_\zeta C^+ \times)][I + \Delta\tau(\delta_\xi A^- \times + \delta_\eta B^- \times + \delta_\zeta C^- \times)]\Delta Q^n = -\Delta\tau R^n \tag{6}$$

where

$$R^n = (\delta_\xi F^n + \delta_\eta G^n + \delta_\zeta H^n + \delta_\eta S_v^n) \tag{7}$$

and the flux Jacobians are defined as

$$A^+ = \frac{\partial F^+}{\partial Q} \tag{8}$$

similarly for A^-, B^+, B^-, C^+, and C^-.

The explicit treatment of the viscous flux vector is referred to as time-lagged viscous terms. This implementation maintains the solution algorithm efficiency of the original Euler algorithm (average increase in computational time is less than 10% for the same grid). Gatlin[6] has shown this algorithm to give reasonable engineering solutions for high Reynolds number flows when used with the Steger-Warming[4] FVS scheme for stationary grids. This treatment of the diffusive terms was applied to the FDS scheme in the work shown here. The method used to evaluate the viscous flux terms has been described in detail by Gatlin[6] and is not repeated here.

The inviscid flux terms can be evaluated according to van Leer et al.[11] in the form

$$F_{i+1/2} = {}^1/_2 (F_i + F_{i+1}) - {}^1/_2 D(Q_i, Q_{i+1}) \times (Q_{i+1} - Q_i) \tag{9}$$

and the freedom of choosing a numerical flux formula essentially lies in the choice of the matrix coefficient, $D(Q_i, Q_{i+1})$, of the dissipation term. The FDS scheme used in this work was based on Roe's[5] approximate Riemann solver, which uses an intermediate state of the dependent variables $\bar{Q}$ to determine the matrix coefficient $\bar{A}(\bar{Q})$ of the dissipation term described in Eq. (9). The first-order numerical flux formula for the Roe-type scheme is

$$F_{i+1/2} = {}^1/_2 (F_i + F_{i+1}) - |\bar{A}|_{i+1/2} (Q_{i+1} - Q_i) \tag{10}$$

Roe[5] required the matrix $\bar{A}(Q_i, Q_{i+1})$ to have certain properties, which he calls Property U, to ensure uniform validity across discontinuities.

The dissipation matrix corresponding to the Steger-Warming splitting (FVS) has been shown to contain too much numerical dissipation. The eigenvalues of the dissipation matrix for the FVS scheme become discontinuous at a flow discontinuity, whereas the eigenvalues of the dissipation matrix for the FDS scheme approach zero at flow discontinuity, resulting in sharp modeling of shocks or contact discontinuities.

The FDS scheme used has been described in detail by Whitfield et al.[3] for application to the three-dimensional Euler equations. The flux formulas shown in Eq. (10) can be extended easily to three dimensions by splitting the wave into the three curvilinear coordinate directions since the eigenvalues are dependent on the contravariant velocities normal to a cell face. The wave motions are split based on these eigenvalues, resulting in a set of equations in which the wave motion is normal to the cell interface just as though they were a set of one-dimensional equations.

The Jacobian matrix $\bar{A}(Q_i, Q_{i+1})$ is evaluated using a set of special Roe-averaged variables for the three-dimensional Euler equations. These are

$$\rho = \sqrt{\rho_i \rho_{i+1}} \tag{11a}$$

$$u = \frac{\sqrt{\rho_i}u_i + \sqrt{\rho_{i+1}}u_{i+1}}{\sqrt{\rho_i} + \sqrt{\rho_{i+1}}} \tag{11b}$$

$$v = \frac{\sqrt{\rho_i}v_i + \sqrt{\rho_{i+1}}v_{i+1}}{\sqrt{\rho_i} + \sqrt{\rho_{i+1}}} \tag{11c}$$

$$w = \frac{\sqrt{\rho_i}w_i + \sqrt{\rho_{i+1}}w_{i+1}}{\sqrt{\rho_i} + \sqrt{\rho_{i+1}}} \tag{11d}$$

$$a^2 = \frac{\gamma p}{\rho} = (\gamma - 1)h - \frac{1}{2}(u^2 + v^2 + w^2) \tag{12a}$$

$$e = \frac{p}{\gamma - 1} + \frac{1}{2}\rho(u^2 + v^2 + w^2) \tag{12b}$$

where h is the total enthalpy.

The details of an implicit algorithm using the FDS is given by Simpson.[7] As noted by Whitfield et al.,[3] the implicit portion of the FDS algorithm has the same form as the implicit portion of the FVS and improved results and convergence rates can be obtained by solving the FVS implicit portion combined with the FDS representation for the residual vector. The reason for the improved results using the implicit portion of the FVS scheme is that approximated flux Jacobians are used for the FDS scheme, whereas the FVS scheme uses the true partials of the flux split Jacobians. Any approximations for these flux Jacobian terms have nearly always degraded the convergence rates of the solution. Therefore, the resulting equation is

$$[I + \Delta\tau(\delta_\xi A^+ \times + \delta_\xi A^- \times + \delta_\eta B^+ \times + \delta_\eta B^- \times + \delta_\zeta C^+ \times + \delta_\zeta C^- \times)]\Delta Q^n = -\Delta\tau R^n \tag{13}$$

$$R^n = (\delta_\xi \bar{F}^+ + \delta_\xi \bar{F}^- + \delta_\eta \bar{G}^+ + \delta_\eta \bar{G}^- + \delta_\zeta \bar{H}^+ + \delta_\zeta \bar{H}^-) \tag{14}$$

The higher order (second and third) numerical fluxes used here are due to Osher and Chakravarthy.[19] The implementation of the higher order methods is described by Whitfield et al.[3] [refer to Eq. (54) in Ref. 3].

Using the equation for the first-order flux, a second- or third-order scheme for the flux at cell interface $i + 1/2$ may be obtained by adding a correction term. If all Roe variables and metric terms used in computing the eigenvalues and eigenvectors are evaluated at the cell face $i + 1/2$, then the higher order flux formula becomes

$$\bar{F}_{i+1/2} = F(Q_i)_{i+1/2} + \sum_{j=1}^{m} \sigma^-_{j,i+1/2} r^j_{i+1/2} + \sum_{j=1}^{m} \left\{ \frac{1 - \Psi}{4} [L_j^+(-1, 1) - L_j^-(3, 1)] + \frac{1 + \Psi}{4} [L_j^+(1, -1) - L_j^-(1, 3)] \right\} r^j_{i+1/2} \tag{15}$$

where

$$\sigma^{\pm}_{j,i+(p/2)} = \lambda^{\pm j}_{i+1/2} \alpha_{j,i+(p/2)} \tag{16}$$

$$\alpha_{j,i-1/2} = l^j_{i+1/2}(Q_i - Q_{i-1}) \tag{17a}$$

$$\alpha_{j,i+1/2} = l^j_{i+1/2}(Q_{i+1} - Q_i) \tag{17b}$$

$$\alpha_{j,i+3/2} = l^j_{i+1/2}(Q_{i+2} - Q_{i+1}) \tag{17c}$$

Two flux limiters were tested in this work; they are defined as the minmod and superbee limiters.[7] All of the turbulent solutions obtained used a modified Baldwin-Lomax turbulence model.[6]

Steady Results

Van Leer et al.[11] and Gatlin[6] have pointed out that the numerical dissipation for the FVS scheme is too large to allow the accurate modeling of flow discontinuities such as shocks and boundary layers. In order to document the effects of numerical dissipation for viscous flow solutions, several steady configurations were tested to compare the FDS scheme with the FVS scheme.

The first configuration was a laminar flat plate boundary-layer calculation for Mach = 0.5 and a Reynolds number based on plate length of $Re = 10^4$. Flow solutions for a laminar boundary layer on a flat plate were obtained using two grids. Both grids used 70 points in the freestream direction. The two grids differed in the number of grid lines in the normal direction from the plate and in the spacing set for the first point off the plate. The first grid used 20 points in the normal direction with the first point off the plate set at 0.002 plate length (fine grid), whereas the second grid used 15 points in the normal direction, and the first spacing was 0.02 plate length (course grid).

The laminar boundary-layer profiles are presented in Fig. 1 for the FDS scheme on the course grid, and FVS on both the course and fine grids. The calculations are shown compared with the Blasius solution for a laminar flat plate. The FDS scheme matches very well with the Blasius solution using the course grid. Note that the FDS scheme has very accurately modeled the laminar boundary-layer profiles with only three mesh points internal to the boundary layer. The fine grid results with the FVS scheme do not compare well with the Blasius solution and the course grid results are even worse. Additional grid refinements did not improve the FVS results. The FVS scheme has too much numerical dissipation to capture the laminar boundary-layer profile, even on a very fine grid.

The RAE 2822 airfoil was used as a check case for the TLNS algorithms using both FDS and FVS. The RAE 2822 was selected because of the experimental data[20] that exists for pressure, skin friction, and velocity profiles. All solutions obtained[7] showed very favorable comparisons for the FDS scheme and experimental data and confirmed the results of Gatlin[6] and van Leer et al.[11] concerning the excessive numerical dissipation of the FVS scheme. The ONERA M6 wing was used as a three-dimensional check case for the FDS scheme. Again, very favorable comparisons were obtained with experimental data. These results are not shown here in order to save space for the more important unsteady results.

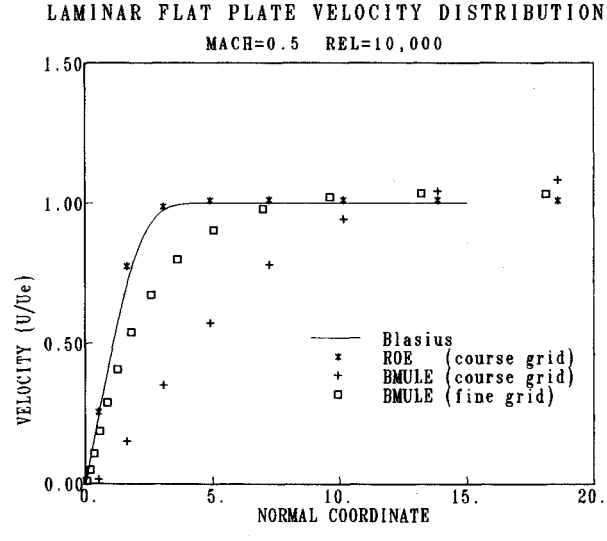

Fig. 1 Velocity profiles for laminar flat plate.

The LRPS wing was used for the three-dimensional unsteady test case due to the extensive amount of wind-tunnel test data[21] that exist. Therefore, for completeness, the LRPS steady results will be presented. However, only FDS minmod second-order results were obtained for the LRPS configuration. The LRPS wing has an aspect ratio of 2 and a rectangular planform. The experimental data used was taken in Freon, and therefore, the ratio of specific heats is $\gamma = 1.131$ with a transonic Mach number of 0.7 and a steady angle of attack of 4 deg.

The grid for this case had 221 points in the streamwise, x-coordinate direction, 40 points normal to the surface, y-coordinate direction, and 15 points in the spanwise, z-coordinate direction. The grid used a C mesh in the streamwise direction and an H mesh in the spanwise direction. Each of the K planes (constant spanwise location) have the same point distribution, with clustering at the leading and trailing edges, Fig. 2. The distribution was selected to give the most orthogonal grid possible. There are 10 K planes distributed along the wing span, with the planes being clustered near the tip. The wingtip was not modeled, instead the airfoil was simply collapsed to a line at the $K = 11$ plane, which was placed just out from the wingtip. An additional four grid planes were distributed in the spanwise direction to the far-field boundary. The spacing for the first point off the wing was set such that a minimum Y^+ of 1.5 occurred on the wing.

The grid described was used for steady calculations to compare with the experimental data[21] to verify the quality of the grid before performing the unsteady calculations. The results near the wingtip are of particular interest since the grid used did not model the tip correctly. The transonic flow conditions were Mach = 0.701 and 4.0-deg angle of attack, which was considerably different from the supercritical design conditions of Mach = 0.8 and 0.0-deg angle of attack, and resulted in a sharp shock near the 20% chord location. Figures 3 and 4 show pressure coefficient chordwise distributions for two span locations, 34% and 95%, respectively. Excellent agreement with the experimental data is evident and confirms the adequacy of the grid (including the collapsed wingtip) and the algorithm to model the flowfield for three-dimensional flows. Belk[2] has reported a predicted shock position downstream of the position shown in the experimental data using an inviscid approximation. The inclusion of the viscous terms has corrected the position of the predicted shock to more nearly coincide with the experimental data.

Unsteady Results

Calculations of unsteady aerodynamics require a time-accurate numerical scheme in which each grid cell is advanced in time an equal amount (i.e., minimum time stepping). The size of a time step is limited by the CFL condition. The use of minimum time steps is very expensive for viscous solutions since grid cells near solid surfaces are very small compared to grid cells in outer regions of the flowfield (6–7 orders of magnitude difference in cell volumes can exist). This means very small time steps must be used over the entire flowfield for minimum time stepping to maintain a reasonable maximum CFL in the grid cells near solid surfaces. If a maximum CFL of 100 is occurring in the grid cells near a solid surface, then most of the flowfield is being advanced in time with CFLs of much less than 1 ($CFL \cong 1 \times 10^{-4} \rightarrow 1 \times 10^{-5}$).

The test cases used to study the effect of CFL on stability and time accuracy were the NACA 0012 airfoil oscillating in pitch about its 25% chord point in transonic conditions and the LRPS wing oscillating in pitch about its 40% chord location. The angle of attack was varied according to

$$\alpha(t) = \alpha_0 + \alpha_u \sin(\hat{\omega}\hat{t}) \tag{18}$$

Unsteady viscous calculations were obtained for the NACA 0012 airfoil at conditions to match the experiment by Landon,[22] with a Mach number of 0.755, mean angle of attack α_0 of 0.016 deg, an unsteady angle of attack amplitude α_u of 2.51 deg, and a reduced frequency or Strouhal number k of 0.1628 based on chord length

$$k = (\hat{\omega}\hat{c})/\hat{V}_\infty \tag{19}$$

where $\hat{\omega}$ is the frequency, $\hat{c}$ the chord length, and $\hat{V}_\infty$ the freestream velocity.

Solutions were obtained for different time step sizes to determine the effects of large CFL numbers on unsteady viscous calculations. All of the NACA 0012 calculations presented were obtained using a C-type numerical grid with 221 × 40 points and a chordwide distribution of points, as shown in Fig. 5. The spacing set for the first point off the body was 1×10^{-6},

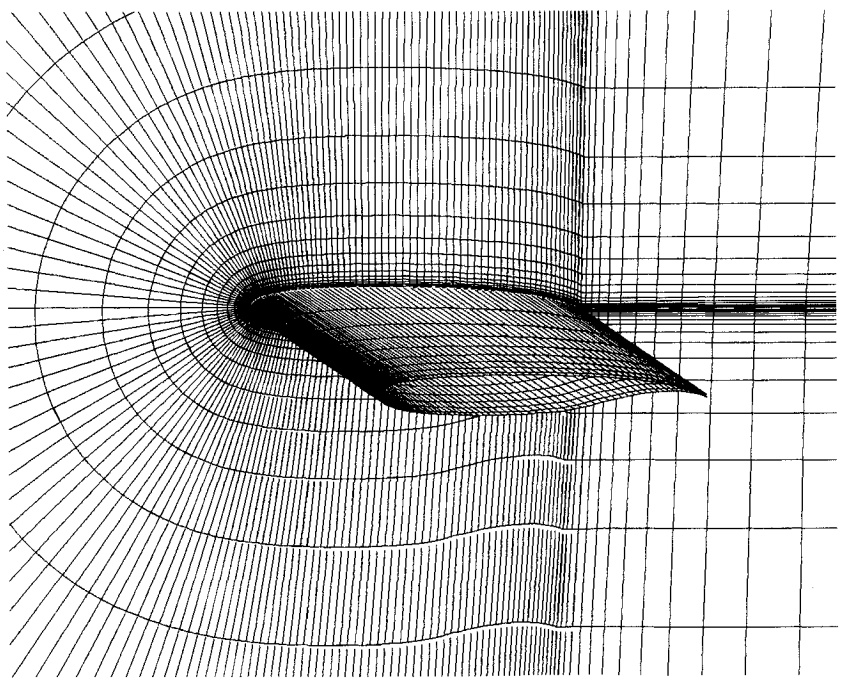

Fig. 2 C-H grid for Langley rectangular planform supercritical wing (221 × 40 × 15).

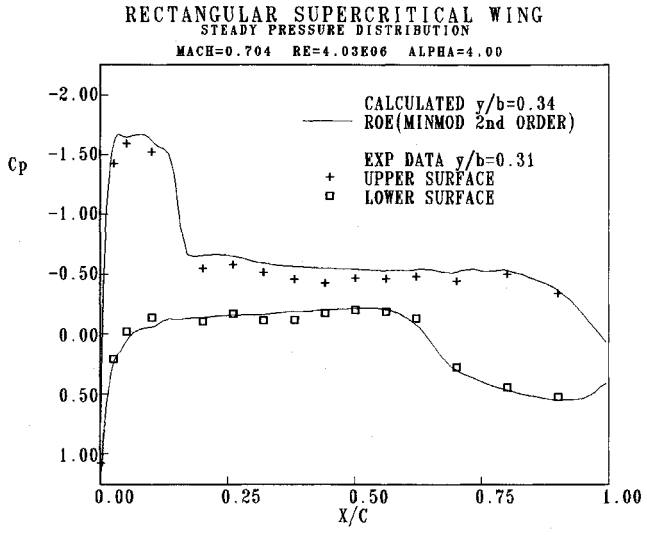

Fig. 3 LRPS wing steady pressure coefficient distributions at 34% span.

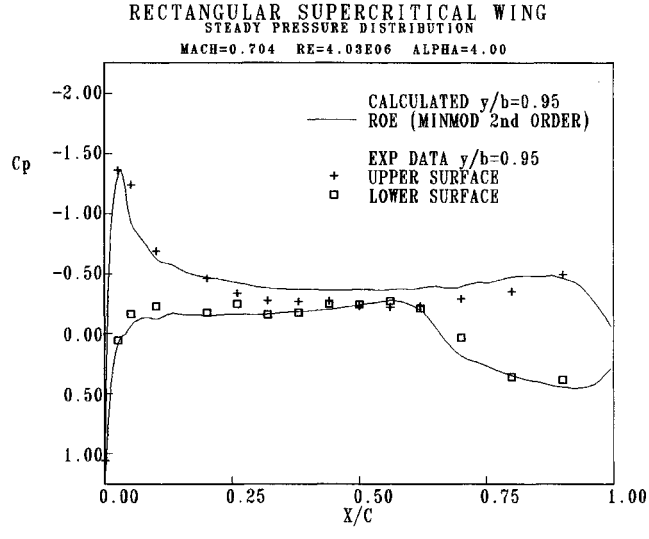

Fig. 4 LRPS wing steady pressure coefficient distributions at 95% span.

which gave approximately 15–20 grid cells inside the boundary layer and resulted in a minimum Y^+ of 0.1 over the entire airfoil.

The unsteady calculations were performed by first obtaining a steady solution for the airfoil at the mean angle of attack, $\alpha_0 = 0.016$ deg. The motion was impulsively started with the angle of attack varied according to Eq. (18). The entire grid was oscillated as a rigid body. The pressure distributions for several different time step sizes are presented in Fig. 6. These pressure distributions are "snapshots" of the pressure in time as the airfoil is in motion. The airfoil is at the 60-degrees-of-motion point, which corresponds to an increasing angle of attack through 2.20 deg. The small time step size $DT = 0.00102$ was used as a reference time step to compare with other results in order to check for time accuracy. As the time step increases, the solution deteriorates to the point of being unusable even though the solution did not "blowup" and continued for a complete cycle of motion.

The time step size $DT = 0.00102$ resulted in 49,500 time steps per cycle of oscillatory motion, whereas a time step size $DT = 0.0511$ required 1002 time steps per cycle of motion and resulted in a maximum CFL of 45,000 for the fine viscous grid. Therefore, the results shown in Fig. 6 indicate that, if unsteady viscous calculations for the oscillating airfoil are to be practical or affordable, additional considerations must be made to reduce computational efforts. Large time steps are possible in the present approach due primarily to the favorable stability properties of the two-pass scheme, as discussed by Anderson,[23] and due to the use of Newton iterations to converge the solution at each time step before updating to the next time step. These Newton iterations, referred to here as subiterations, have been tried successfully by others (see Ref. 15), but not with the FDS algorithm described here, not with an explicit treatment of the viscous terms, and not with Jacobian freezing.

The implementation of subiterations into the scheme is simply the addition of a term to the right side of Eqs. (13) and (14) and a redefinition of ΔQ^n on the left side:

$$[I + \Delta\tau(\delta_\xi A^+ \times + \delta_\eta B^+ \times + \delta_\zeta C^+ \times)] \times [I + \Delta\tau(\delta_\xi A^- \times + \delta_\eta B^- \times + \delta_\zeta C^- \times)]\Delta Q^p = -\Delta\tau R^p \tag{20a}$$

$$-\Delta\tau R^p = -\Delta\tau\left[\frac{Q^p - Q^n}{\Delta\tau} + (\delta_\xi F^p + \delta_\eta G^p + \delta_\zeta H^p + \delta_\eta S_v^p)\right] \tag{20b}$$

where ΔQ^p is defined as

$$\Delta Q^p = Q^{p+1} - Q^p \tag{20c}$$

where p is the subiteration count. When $p = 0$, $Q^p = Q^n$, and the system reverts to the noniterative scheme of Eq. (13). At convergence, $Q^p \to Q^{n+1}$. Note that in this case the viscous terms are no longer time lagged.

Ortega and Rheinboldt[24] have shown that flux Jacobians can be frozen (not updated) during a Newton iteration. The significance of freezing the Jacobians and the resulting simplified Newton method is a tremendous savings in computations since the cost to recalculate the flux Jacobians is between 40–45% of the cost of doing an entire iteration. Both methods, with and without Jacobian freezing, were tried with no noticeable differences in the results; therefore, only the simplified Newton method results are shown.

Pressure distributions for the NACA 0012 at 60 degrees motion are shown in Fig. 7 for time step size $DT = 0.0511$. The pressure distribution shows some moderate wiggles for the zero subiterations, whereas for only four subiterations, the solution is much smoother and is suitable for determining the lift and moment coefficients for use in design and analysis studies. There is no noticeable difference between 4 subiterations and 16.

The idea of using subiterations for unsteady calculations was to converge the solution at each time step and therefore allow for much larger time steps sizes. However, problems exist for converging solutions with numerical grids designed for viscous flows that have a large variation in grid cell aspect ratio between grid cells near a solid surface and grid cells in the far field. A possible solution for the convergence rate problem during subiterations is the use of local time stepping.

Local time steps for subiterations were implemented such that the overall time accuracy of the minimum time step iterations was preserved. Equation (20b) then becomes

$$-\Delta\tau R^p = -\Delta\tau_{\text{local}}\left[\frac{Q^p - Q^n}{\Delta\tau_{\min}} + (\delta_\xi F^p + \delta_\eta G^p + \delta_\zeta H^p + \delta_\eta S_v^p)\right] \tag{21}$$

The result of using local subiterations, Eq. (21), was a significant increase in the convergence rate for subiterations as long as the CFL for the local subiterations was small enough to maintain stability. Numerical experiments showed that the local CFL must usually be less than 1.

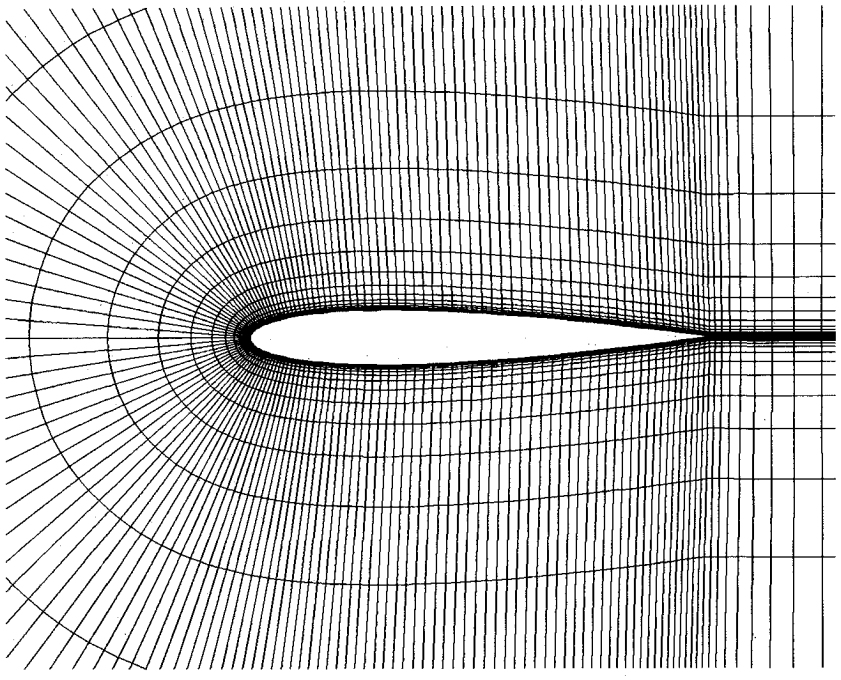

Fig. 5 C grid for NACA 0012 airfoil (221 × 40 × 2).

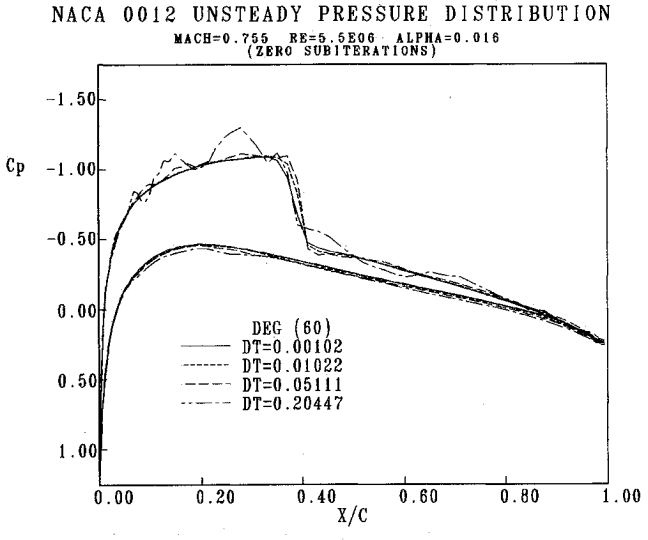

Fig. 6 NACA 0012 unsteady pressure coefficient distributions for different time step sizes.

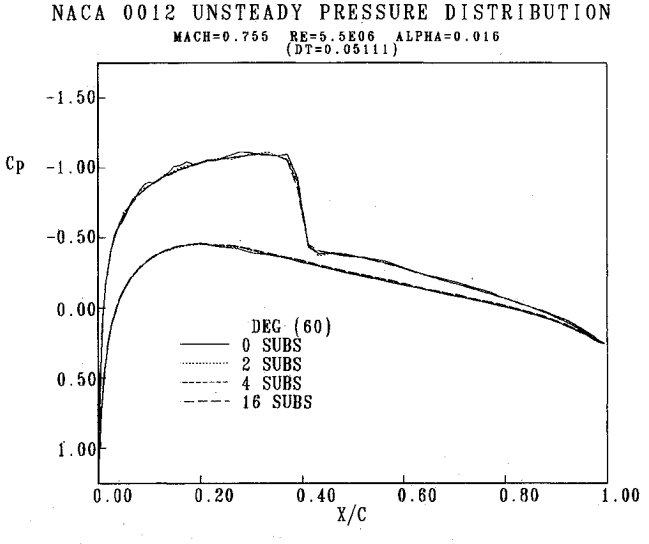

Fig. 7 NACA 0012 unsteady pressure coefficient distributions using minimum time step subiterations, DT = 0.0511.

The pressure distributions in Fig. 8 show very smooth results for time step size DT = 0.05111 using local time step subiterations even for only two subiterations. There is no noticeable difference in the solutions between two local time step subiterations and four local time step subiterations.

Time-accurate calculations with this algorithm would at first glance seem to be limited to first-order temporal accuracy. However, the use of subiterations alleviates this problem because linearization and factorization errors go to zero at convergence. Therefore, using a second-order time discretization with subiterations gives a second-order accurate in time scheme at convergence. A comparison of a first- and second-order temporal differencing with DT = 0.0511 was obtained for four cycles of motion (1440 degrees of oscillatory motion) of the NACA 0012. Figure 9 shows "snapshots" of the unsteady pressures using DT = 0.0511 and four subiterations for first- and second-order temporal accuracy compared with DT = 0.00511 and zero subiterations and with the experimental data.[22]

In Fig. 9a, the shock location of the second-order solution is leading the shock location predicted by the first-order solutions for DT = 0.005111 and 0.05111 with four minimum subiterations. The largest difference occurs when the shock is traveling the fastest, such as the 70 degrees of oscillatory motion (Fig. 9b). Note that at the point where the shock is basically stationary (i.e., 160 degrees of motion, Fig. 9c) the two DT = 0.05111 cases for first- and second-order temporal schemes are essentially identical.

The three-dimensional unsteady calculations were obtained for the LRPS wing at a Mach number of 0.699 and a steady angle of attack of 4.03 deg. The angle of attack was varied according to Eq. (18) with an unsteady amplitude of 1.035 deg and a reduced frequency, Eq. (19), of 0.358.

A steady starting condition was obtained using a CFL of 5 for 1000 iterations, after which the motion was impulsively started. The calculations were run for three cycles of motion. During the third cycle, the pressure coefficients were saved at each time step. The time step size was DT = 0.069, which

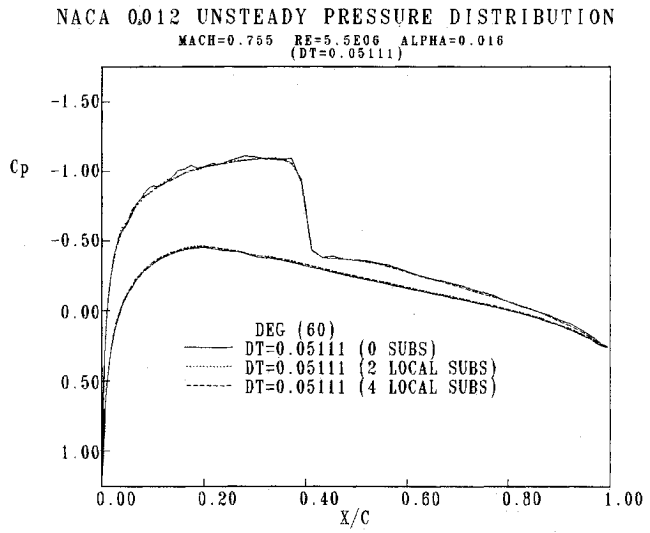

Fig. 8 NACA 0012 unsteady pressure coefficient distributions using local time step subiterations, $DT = 0.0511$.

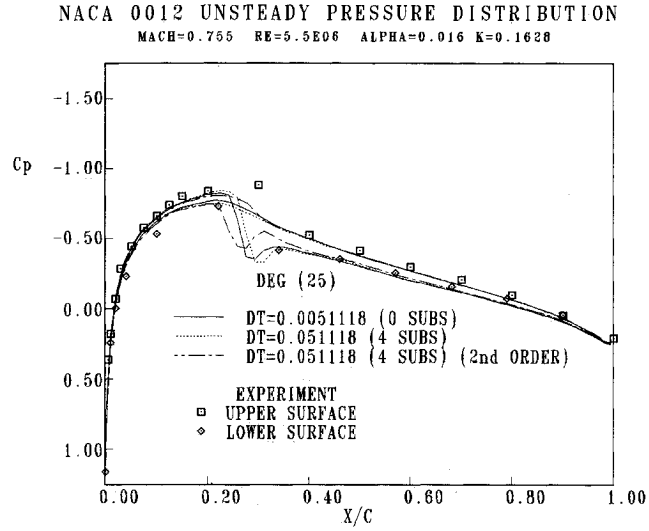

Fig. 9a Unsteady pressure coefficient distributions for first- and second-order time accuracy, 25 degrees of motion.

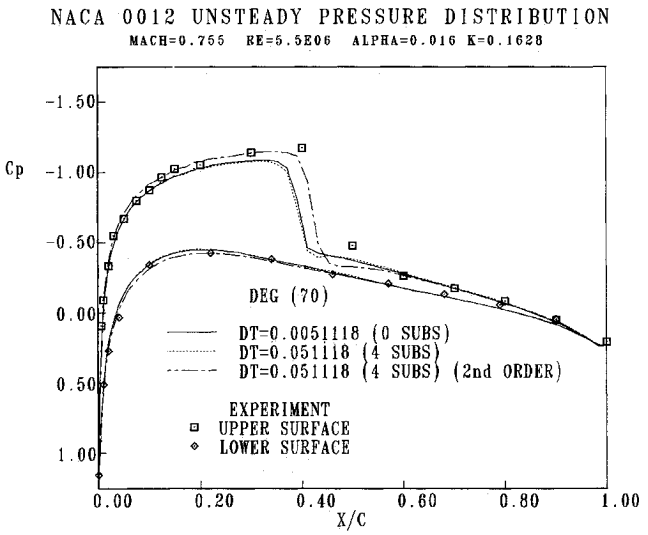

Fig. 9b Unsteady pressure coefficient distributions for first- and second-order time accuracy, 70 degrees of motion.

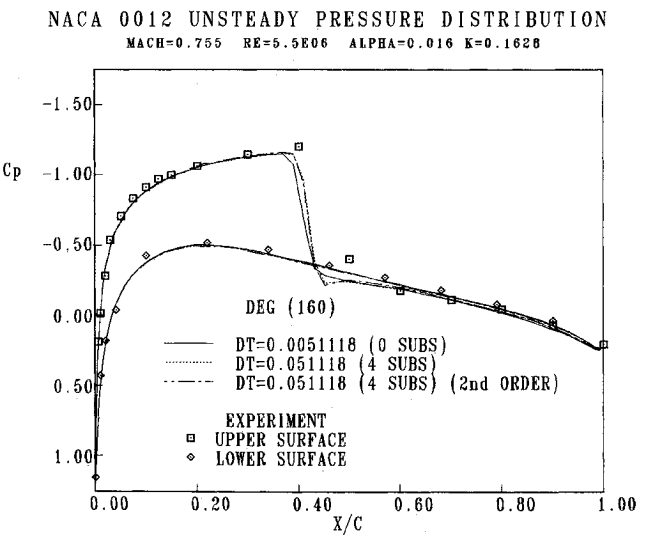

Fig. 9c Unsteady pressure coefficient distributions for first- and second-order time accuracy, 160 degrees of motion.

corresponds to 360 time steps per cycle of motion (same as used by Belk[2] for the inviscid calculations), and five minimum time step subiterations were used to converge the solution at each time step by nearly one order of magnitude. The maximum CFL for this case was approximately 17,000.

The magnitude and phase of the unsteady pressure coefficients from the third cycle of motion was obtained by Fourier analysis. The magnitude and phase of the unsteady pressure coefficients are presented along with the inviscid results from Belk[2] and the experimental data[21] for the semispan locations in Figs. 10a–10d. Again, the predicted results compare well with the experimental data. Belk[2] reported a misplacement of the sharp spike in magnitude of the unsteady pressure coefficient due to the inviscid code misplacing the shock. Once again, the inclusion of the viscous terms has seemingly corrected this problem to give good agreement with the experimental data, as shown in Figs. 10a and 10b.

The agreement with experimental data tends to degrade near the wingtip, such that at the 95% semispan location the phase comparison (Figs. 10c and 10d) is not as good. The shift in the phase for the upper surface is obviously misplaced, and the phase for the lower surface is consistently under predicted. The story is similar but not as severe at 85% semispan location (not shown here). The reduced accuracy at the tip should come as no great surprise considering the grid treatment of the wingtip. The inviscid solutions shown from Belk[2] were obtained using a C-O-type wing grid in which the actual wingtip was modeled by wrapping the grid around the tip. This more accurate treatment of the wingtip explains the improved results obtained from the Euler code at the tip.

These results required nearly 6 h of CPU time per cycle of motion on Cray-2, which demonstrates that unsteady viscous calculations are still very expensive. However, it is estimated that the cost of these calculations, without the use of Newton subiterations and Jacobian freezing, would have been approximately 200 CPU h per cycle of motion. This comparison demonstrates that the technique, although still expensive, results in a significant improvement in CPU time.

Conclusions

An algorithm has been presented for computing unsteady thin-layer Navier-Stokes solutions for oscillating airfoils and wings. The FDS algorithm was first compared with the FVS algorithm for steady viscous calculations. The computer laminar boundary-layer profiles for a flat plate were compared with the Blasius solutions, and the FDS was the clear winner since it managed to capture the laminar profile with only three grid

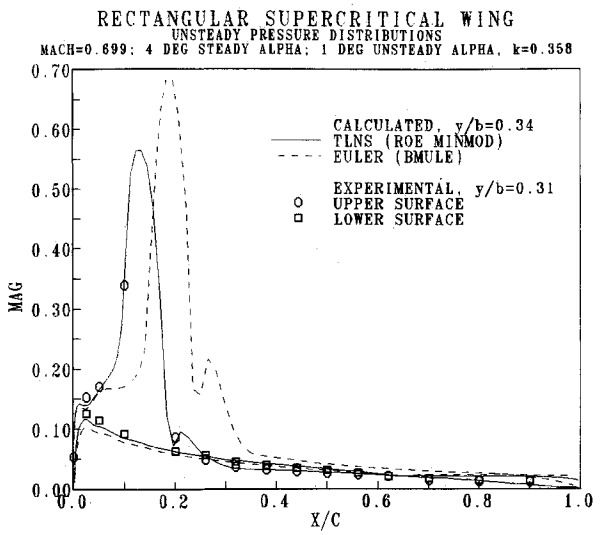

Fig. 10a Magnitude of unsteady LRPS wing pressure distributions at 34% span.

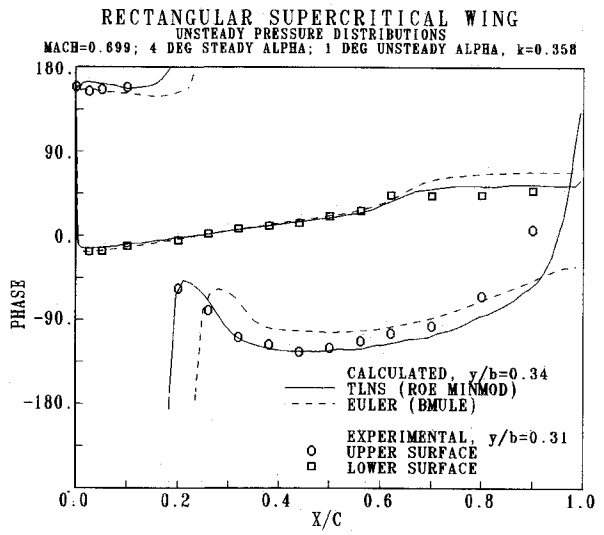

Fig. 10b Phase of unsteady LRPS wing pressure distributions at 34% span.

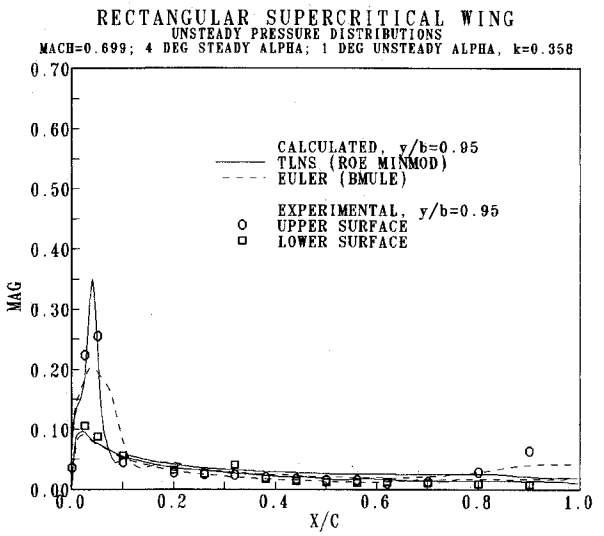

Fig. 10c Magnitude of unsteady LRPS wing pressure distributions at 95% span.

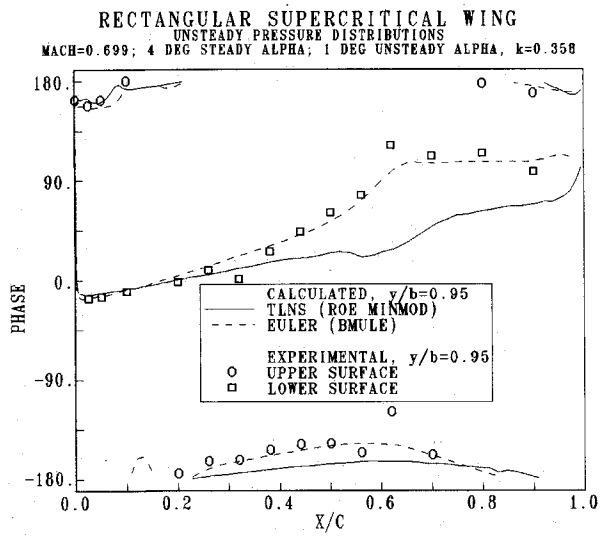

Fig. 10d Phase of unsteady LRPS wing pressure distributions at 95% span.

points inside the boundary layer; whereas with four times as many grid points inside the boundary layer, the FVS scheme still could not match the comparison of FDS with the Blasius solutions. The excess numerical dissipation in the FVS scheme is also observed in shocks in the form of smearing the shock waves over several grid cells. The improved solutions for the FDS scheme did not come cheap since the FDS scheme has a higher operational count than does the FVS (approximately 20% higher) and the convergence rate for the FDS scheme is slower than the FVS scheme, therefore requiring more iterations to reach the same convergence level (approximately 25% more iterations).

The second-order FDS scheme with the minmod limiter was selected as the algorithm to be used for the unsteady thin-layer Navier-Stokes computations. The emphasis was placed on obtaining time-accurate viscous solutions for oscillating airfoils and wings as cheaply as possible. Since the diffusive terms were treated explicitly, the formal temporal accuracy of the algorithm without subiterations was limited to first-order accurate. A form of Newton subiterations was implemented to converge the unsteady calculations at each time step before progressing the solution to the next time step. The use of these subiterations then allowed the calculations to progress at much larger time step sizes (and CFL number) than would otherwise be possible. The use of subiterations also provided the capability for a second-order time-accurate scheme at convergence of the subiterations.

The use of subiterations were shown to significantly improve the quality of the solution and, in some cases, allow a solution to be obtained that otherwise would have been impossible at the time step size being used. Unsteady calculations for the two-dimensional NACA 0012 airfoil were performed to help select the proper combinations of the step size and subiteration number to give the best possible solution. The results from these calculations were used to make more extensive two- and three-dimensional unsteady calculations to compare with experimental data. The three-dimensional calculations for the supercritical rectangular planform wing showed excellent agreement with the experimental data, and the use of subiterations with the FDS scheme resulted in a relatively efficient algorithm that could be used in more complex three-dimensional unsteady viscous calculations.

References

[1]Arabshahi, A., "A Dynamic Multi-Block Approach to Solution of the Three-Dimensional Time-Dependent Euler Equations About Complex Configurations," Ph.D. Dissertation, Mississippi State Univ., Mississippi State, MS, May 1989.

[2]Belk, D. M., "Unsteady Three-Dimensional Euler Equations Solutions on Dynamic Blocked Grids," Ph.D. Dissertation, Mississippi State Univ., Mississippi State, MS, Aug. 1986.

[3]Whitfield, D. L., Janus, J. M., and Simpson, L. B. "Implicit Finite Volume High Resolution Wave-Split Scheme for Solving the Unsteady Three-Dimensional Euler and Navier-Stokes Equations on Stationary or Dynamic Grids," Mississippi State Univ., Rept. MSSU-EIRS-ASE-88-2, Mississippi State, MS, Feb. 1988.

[4]Steger, J. L., and Warming, R. F., "Flux Vector Splitting of the Inviscid Gasdynamic Equations with Application to Finite-Difference Methods," *Journal of Computational Physics,* Vol. 40, No. 2, 1981, pp. 263–293.

[5]Roe, P. L., "Approximate Riemann Solvers, Parameter Vector, and Difference Schemes," *Journal of Computational Physics,* Vol. 43, No. 2, 1981, pp. 357–372.

[6]Gatlin, B., "An Implicit, Upwind Method for Obtaining Symbiotic Solutions to the Thin-Layer Navier-Stokes Equations," Ph.D. Dissertation, Mississippi State Univ., Mississippi State, MS, Aug. 1987.

[7]Simpson, L. B., "Unsteady Three-Dimensional Thin-Layer Navier-Stokes Solutions on Dynamic Blocked Grids," Ph.D. Dissertation, Mississippi State Univ., Mississippi State, MS, Dec. 1988.

[8]Whitfield, D. L., "Implicit Upwind Finite-Volume Scheme for the Three-Dimensional Euler Equations," Mississippi State Univ., Rept. MSSU-EIRS-ASE-85-1, Mississippi State, MS, Sept. 1985.

[9]Lijewski, L. E., "Transonic Flow Solutions on a Blunt, Body-Wing-Canard Configuration Using an Explicit Euler Solver," 5th Applied Aerodynamics Conf., AIAA Paper 87-2273, Monterey, CA, Aug. 1987.

[10]Belk, D. M., and Whitfield, D. L., "Time-Accurate Euler Equation Solutions on Dynamic Blocked Grids," *Proceedings of the 8th Computational Fluid Dynamics Conference,* AIAA Paper 87-1127, AIAA, New York, June 1987, pp. 292–302.

[11]Van Leer, B., Thomas, J. L., Roe, P. L., and Newsome, R. W., "A Comparison of Numerical Flux Formulas for the Euler and Navier-Stokes Equations," *Proceedings of the AIAA 8th Computational Fluid Dynamics Conference,* AIAA Paper 87-1104, pp. 36–39.

[12]Chakravarthy, S. R., and Osher, S., "A New Class of High Accuracy TVD Schemes for Hyperbolic Conservation Laws," AIAA Paper 85-0363, Jan. 1985.

[13]Janus, J. M., "Advanced 3-D CFD Algorithm for Turbomachinery," Ph.D. Dissertation, Mississippi State Univ., Mississippi State, MS, May 1989.

[14]Lijewski, L. E., "Transonic Euler Solutions on Mutually Interfering Finned Bodies," AIAA 27th Aerospace Sciences Meeting, AIAA Paper 89-264, Reno, NV, Jan. 1989.

[15]Rai, M. M., and Chakravarthy, S. R., "An Implicit Form for the Osher Upwind Scheme," *AIAA Journal,* Vol. 24, No. 5, May 1986, pp. 735–743.

[16]Pulliam, T. H., and Steger, J. L., "Implicit Finite-Difference Simulations of Three-Dimensional Compressible Flow," *AIAA Journal,* Vol. 18, No. 2, 1980, pp. 159–167.

[17]Briley, W. R., and McDonald, H., "Solution of the Multidimensional Compressible Navier-Stokes Equations by a Generalized Implicit Method," *Journal of Computational Physics,* Vol. 24, No. 4, 1977, pp. 372–397.

[18]Beam, R. M., and Warming, R. F., "An Implicit Finite-Difference Algorithm for Hyperbolic Systems in Conservation Law Form," *Journal of Computational Physics,* Vol. 22, No. 1, 1976, pp. 87–110.

[19]Osher, S., and Chakravarthy, S. R., "Very High Order Accurate TVD Schemes," Inst. for Computer Applications in Science and Engineering, Rept. 84-44, 1984.

[20]Cook, P. J., McDonald, M. A., and Firmin, M. C. P., "Aerofoil RAE 2822-Pressure Distributions and Boundary Layer and Wake Measurements," AGARD-AR-138, May 1979.

[21]Ricketts, R. H., Sandford, M. C., Watson, J. J., and Seidel, D. A., "Subsonic and Transonic Unsteady and Steady-Pressure Measurements on a Rectangular Supercritical Wing Oscillated in Pitch," NASA TM-85765, Aug. 1984.

[22]Landon, R. H., "NACA 0012. Oscillatory and Transient Pitching," *Compendium of Unsteady Aerodynamic Measurements,* AGARD-R-702, Aug. 1982.

[23]Anderson, W. K., "Implicit Multigrid Algorithms for the Three-Dimensional Flux Split Euler Equations," Ph.D. Dissertation, Mississippi State Univ., Mississippi State, MS, Aug. 1986.

[24]Ortega, J. M., and Rheinboldt, W. C., *Iterative Solution of Nonlinear Equations in Several Variables,* Academic, New York, 1970, pp. 181–187.